Int J Adv Manuf Technol (2014) 74:423–432
DOI 10.1007/s00170-014-5999-9

ORIGINAL ARTICLE

The influences of shear deformation on the evolutions of the extrusion shear for magnesium alloy

H.-J. Hu · H. Wang · Z.-Y. Zhai · Y.-Y. Li · J.-Z. Fan · O. U. Zhongwen

Received: 10 April 2014 / Accepted: 20 May 2014 / Published online: 5 June 2014

Abstract A new type of magnesium alloy extrusion-shear (short for ES) composite extrusion technology which combines the characteristics of direct extrusion and two pass equal channel extrusion has been put forward. The experiments of ES process and direct extrusion have been performed, and direct extrusion and ES dies suitable for industrial horizontal extruder have been designed and manufactured. Three-dimensional thermomechanical finite element models and conditions of the ES process and direct extrusion have been established. Extrusion forces and accumulated strains and stresses and temperatures evolution of the ES process have been obtained. The loads of the ES process increase obviously compared with those of direct extrusion. Maximum temperatures during the ES process are higher than those of direct extrusion. The computer simulation analyses of stress state for the billets reveal that part of the billet is exerted in four directions of compressive stress. The ES process could cause cumulative strains and shear stress in magnesium alloy billets than direct extrusion. Therefore, more grain refinements could be achieved. Based on the microstructure observations of center positions for the ES process and direct extrusion rods, grains have been effectively refined with extrusion temperature. It is found that there are many similarities between finite element simulation results and experimental results.

Keywords Wrought magnesium alloy · Extrusion shear · Extrusion force · ES process · Microstructure · Dynamic recrystallization · Stress state

H.-J. Hu (✉) · H. Wang · Z.-Y. Zhai · Y.-Y. Li · J.-Z. Fan
College of Material Science and Engineering, Chongqing University of Technology, 400050 Chongqing, China
e-mail: hhj@cqut.edu.cn

H.-J. Hu · O. U. Zhongwen
PLA Chongqing Logistics Engineering College, 401311 Chongqing, China

1 Introduction

With excellent properties of lightweight, damping, heat conductive, electromagnetic shielding, and so on, magnesium alloy is known as a green material of resource and environment sustainable development in the twenty-first century [1]. But magnesium alloy has close-packed hexagonal crystal structure and less independent slip system at room temperature, which could lead to low plasticity and make it difficult to be deformed.

With regard to close-packed hexagonal crystal structure, the cold plasticity of magnesium is low, and only at a temperature of more than 225 °C that additional gliding planes could be moved. Therefore, magnesium alloy exhibits good plasticity by more compression stress. Wrought magnesium alloys have a special feature. Their compressive proof strength is smaller than tensile proof strength [2, 3]. After forming, wrought magnesium alloys have a stringy texture in the deformation direction, which increases the tensile proof strength. In compression, the proof strength is smaller because of twinning, which happens more easily in compression than in tension for magnesium alloys because of the hexagonal lattice structure. The design idea of extrusion-shear (ES) die is to combine the direct extrusion and continue shearing to increase the compression and shear stresses of the workpiece during the extrusion process, thereby the plasticity of the magnesium alloy can be improved, as well as the stress of the metal-forming process also could increase the plasticity. The strain could be introduced into the samples by ES process. The ES process can be used to produce large strains in the sample. The magnitude of effective strain is achieved by multiplying the magnitude of effective strain in the first pass by the number of shearing. The ES process can be used to control the crystallographic texture of structural bulk ultra-fined grain materials.

Reduction of the processed metals and alloys to the submicron grain size can lead to significant improvements in their mechanical properties, in particular increasing the materials'

tensile strength and yield strength, as well as giving them superplastic capability, which is of great interest to the modern aerospace industry.

Equal channel angular extrusion (ECAE) is an extrusion process developed in the early 1990s in the Soviet Union. The technique is able to refine the microstructure of metals and an alloy, thereby improving their strength according to the Hall–Petch relationship. ECAE is unique because significant cold work can be accomplished without reduction in the cross-sectional area of the deformed workpiece. The ES process combines the direct extrusion and two consecutive shearing according to the characteristics of the ES process.

The two consecutive shearing are path C of the ECAE process shown in Fig. 1. After each pass, a rod is rotated around its longitudinal axis through an angle of 180° (route C).

In this paper, the ES deformation process has been simulated by using the software and finite element method, the extrusion forces and cumulative strains and temperature distribution of the ES process and direct extrusion have been predicted, and the state of stress of the billet has been analyzed. Meanwhile, the ES process and direct extrusion experiments of AZ31 magnesium alloy have been performed. The ES process- and direct extrusion-deformed microstructures with an extrusion ratio of 12 and extrusion temperature of 370 °C have been observed and analyzed. The mechanism of dynamic recrystallization microstructure of the ES process has been analyzed and discussed.

2 Experimental materials and FEM methods

ES experiments were performed on the horizontal extrusion machine with an extrusion cylinder of 85 mm in diameter at the Chongqing University national magnesium alloy center. The billet was as-cast AZ31 magnesium alloy which needed to be heated for 2 h with the die before extrusion to achieve the desired temperature. The commercial AZ31 magnesium alloy ingot was used in the experiment, and its nominal composition (mass fraction) is Al 3 %, Zn 1 %, and Mg margin. After 400 °C×15 h of the homogenization treatment, the ingots were air-cooled and finally were lathed to 80-mm diameters. Numerical analysis and test parameters have been carried out as shown in Table 1. In the experiment, the samples were intercepted in the extrusion direction, and all microstructures were taken from the central portion of the bar. Corroding with acetic acid and picric acid solution (2 ml of acetic acid+1 g picric acid+5 ml water+20 ml of alcohol), the microstructure was observed using the PME OLYMPUS TOKYO type of metallurgical microscope [4, 5].

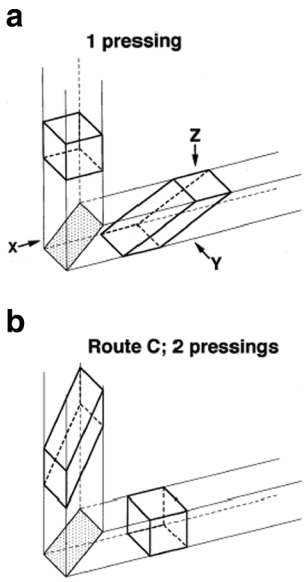

Fig. 1 Schematic illustration of shearing for different routes of ECAE. **a** One pressing. **b** Two pressings with a rotation of 180°

The DEFORM™-3D software package has been employed in the present research. DEFORM is an engineering software that enables designers to analyze metal forming, heat treatment, machining, and mechanical joining processes on the computer rather than the shop floor using trial and error. Process simulation using DEFORM has been instrumental in cost, quality, and delivery improvements at leading companies for two decades. DEFORM™-3D is a powerful process simulation system designed to analyze the three-dimensional (3D) flow in complex metal forming processes. DEFORM-3D is a practical and efficient tool to predict the material flow in industrial forming operations without the cost and delay of shop trials. In this paper, plasticity material has been used for the billet and a rigid material model for the dies. The elastic behaviors of the workpiece and tooling materials have been neglected in these material models. The flow stress–strain data of the AZ31 alloy were input to the module of material library. Parameters used in numerical simulation including material characteristics of the ES process and direct extrusion, billet

Table 1 Main parameters of FEA and experiments

Extrusion ratio	12
Billet length	250 mm
Billet diameter	80 mm
Channel angle	120°
Corner radius	2 mm
Length of die land	4 mm
Die temperature	370 °C
Billet temperature	350 °C
Total number of elements for workpiece	20,000
Mesh density type	Relative
Relative interference depth	0.7
Coefficient of friction	0.4
Extrusion speed	20 mm/s

temperature, the coefficient of friction between the die and the workpiece, etc. are seen in Table 1. The establishments of the finite element model including the workpiece, the punch, and the die model have been established respectively by using 3D modeling software and have been saved as STL file format seen in Fig. 2a, b. Figure 2c presents the schematic diagram of the ES experiments. The parameters of the ES process have been listed in Table 1.

3 Results and discussion

3.1 Evolution of extrusion force for different deformation paths

Curves of the requirement forces varying with time for different deformation paths are described in Fig. 3. Finite element method (FEM) simulation is utilized to indicate the effects of different preheated temperatures on extrusion forces. The extrusion force is important for the design of the die and selection of forming equipment. From Fig. 3, it can be seen that the effects of deformation paths on extrusion force are at ram speeds of 20 mm/s with a billet temperature of 370 °C. From the figures, it can be seen that the ES extrusion might cause the higher extrusion force than direct extrusion. These figures show that adding a shearing of ES extrusion would increase the extrusion load by comparing with direct extrusion.

The ES extrusion process can be obviously divided into four stages compared with the direct extrusion based on varieties of extrusion forces which include stage I, stage II, stage III, and stage IV. The direct extrusion and ES extrusion have overlapped three stages. At the initial stage, the load increases slowly during upsetting phase, but the force increases rapidly due to the work hardening resulting from the continuous accumulation of dislocations and the values of extrusion forces are almost equivalent. The increments of force become slow after 1.2 s, and the force curves are almost parallel with each other when ES extrusion and direct extrusion are in the extrusion steady stage. And the forces of ES

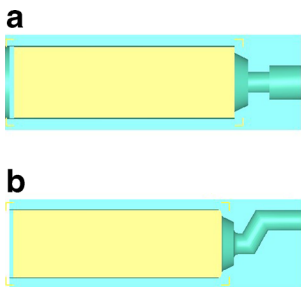

Fig. 2 Diagram of direct extrusion (**a**) and ES die structure (**b**) with conical pre-deformation die with an angle of 50°, and schematic diagram of forming steps with the ES process (**c**)

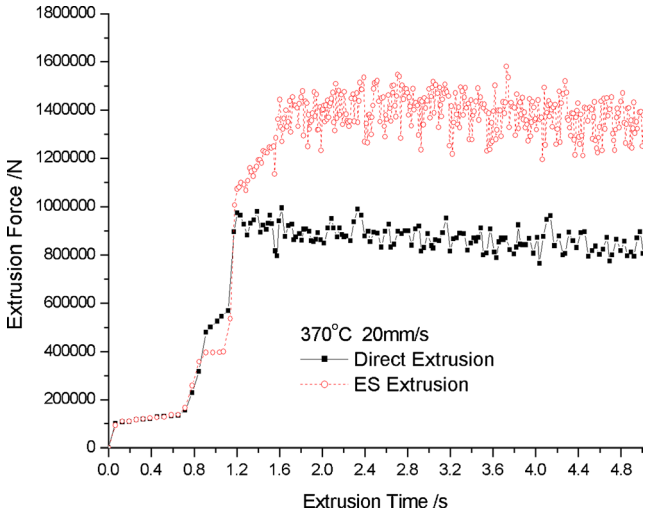

Fig. 3 Force curves of the ES and direct extrusion with an extrusion temperature of 370 °C

extrusion are about 1.6 times as much as those caused by the direct extrusion. During the third phase, the load oscillates an average value of about 1 and 1.6 MN for the direct extrusion and ES processes, respectively. It is clear that extrusion force rises sharply from 0 to about 40 t in stage I. In stage II, the extrusion force increases to about 50 t. In stage III, the extrusion force rises sharply to about 160 t with extrusion punch moving on continually. In this stage, the deformation zone is kept stable, and the extrusion force is slightly fluctuant.

The values of extrusion forces are varying periodically when the deformations are stable. The load-time curves could exhibit the characteristic of strain softening with a peak stress to a steady-state regime, which is a typical phenomenon caused by the dynamic recovery or recrystallization. Deformation paths greatly influence the magnitude of the extrusion force. The extrusion force decreases slightly from the maximum value owing to the gradual reduction of the friction caused by the gradual diminishment of the contact areas between the billet and die.

3.2 Evolution of effective strain evolutions for different deformation paths

In order to gain the deformation characteristics of billets for the ES process and direct extrusion, the predicted effective strain provides quantitative insight into the deformation behavior of the billet during the ES process [6, 7]. Figure 4 shows the effective strain contours of billets, which provided the important information regarding the effective strain distribution. The strain distributions for deformation ways of billets are significantly different. Subpanels a and b of Fig. 4 show the strain distributions for direct extrusion when extrusion times are 0.65 and 1.22 s, respectively. The strain distribution is characterized by symmetry along the extrusion axes in

Fig. 4a, b. The strain value of direct extrusion calculated from Eq. (1) is about 2.5.

$$\varepsilon = \ln\lambda \tag{1}$$

where ε is the accumulative strain, and λ is the extrusion ratio.

Distributions of the strain are lamellar with distinct deformation gradients in Fig. 4c. The deformation of this zone is close to the simple shear deformation in the extrusion time of 1.6 s. From the strain evolutions during the ES process, it can be found that the strains increase with the ES process progressing, the reason being that dynamic recrystallization is taking place.

Figure 4d indicates the strain distributions when the extrusion time is 2 s. It can be found that the minimum and maximum strains rise from 0.043 to 0.053 and 1.08 to 2.69, respectively, compared with the values caused by direct extrusion in Fig. 4b, and the effective strains increase obviously. It indicates that the largest strains exist in the corner region, where the simple shear occurs [8, 9]. The ES process would increase the cumulative strain enormously compared with the direct extrusion. The severe plastic deformation can be obtained by two channels with uniform internal diameter. The distribution patterns are very similar in spite of the fact that the actual values are somewhat different.

The principle of extrusion-shear process is to introduce compressive and accumulated shear strains into the samples. The characteristics of extrusion-shear process are that the sample is subjected to two shearing. Accumulative strain is introduced by a reduction in the cross-sectional area. ECAE produces significant deformation strain without reducing the cross-sectional area. This is accomplished by extruding the workpiece around two corners. The accumulative strains of extrusion shear can be expressed as Eq. (2) which include accumulative strain of direct extrusion and two continuous shearing [4]. The calculated strain value is about 3.82.

$$\varepsilon = \ln\lambda + 2 * \left[\frac{2\cot\left(\frac{\phi}{2}+\frac{\psi}{2}\right) + \psi\csc\left(\frac{\phi}{2}+\frac{\psi}{2}\right)}{\sqrt{3}}\right] \tag{2}$$

where ε is the accumulative strain, λ is the extrusion ratio, Φ is the inner channel angle, and Ψ is the outer channel angle.

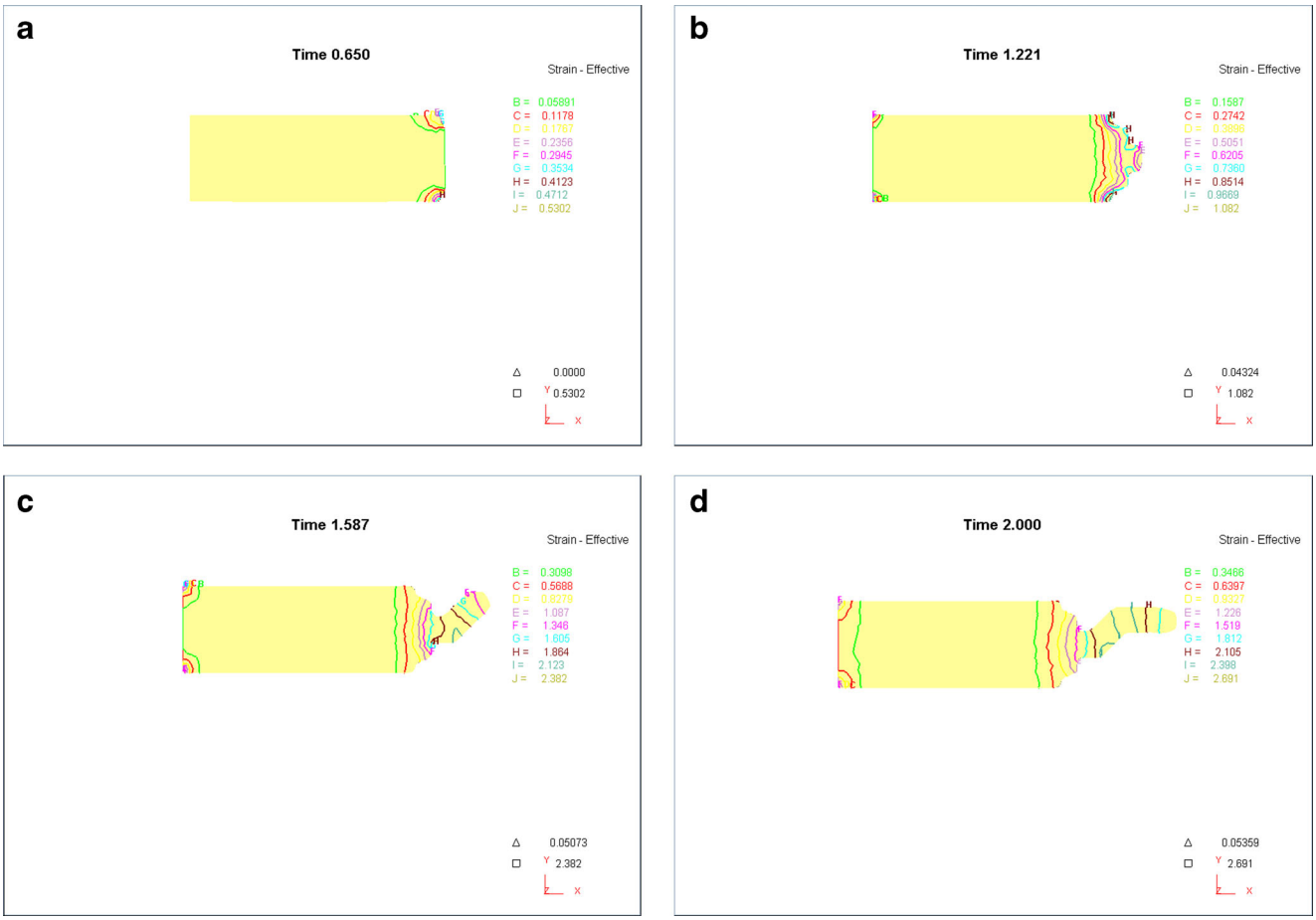

Fig. 4 Effective strain evolution. **a** Phase I. **b** Phase II. **c** Phase III. **d** Phase IV

The multiple shearing of the ES process produce a systematic increase of deformation, leading to a successive decrease in grain size by means of forming first a grid of low-angle and then high-angle boundaries.

Particle tracking method is performed to analyze strain evolution for certain points during extrusion-shear and direct extrusion processes. [4]. To illustrate clearly the strain changing with ram displacement, the strains at selected points "p1," "p2," and "p3" in the billet shown in Fig. 5a have been tracked, and the point p2 is an interior point in the billet center, and the points p1 and p3 are points near the billet surface. The evolutions of effective strains have been shown at these points

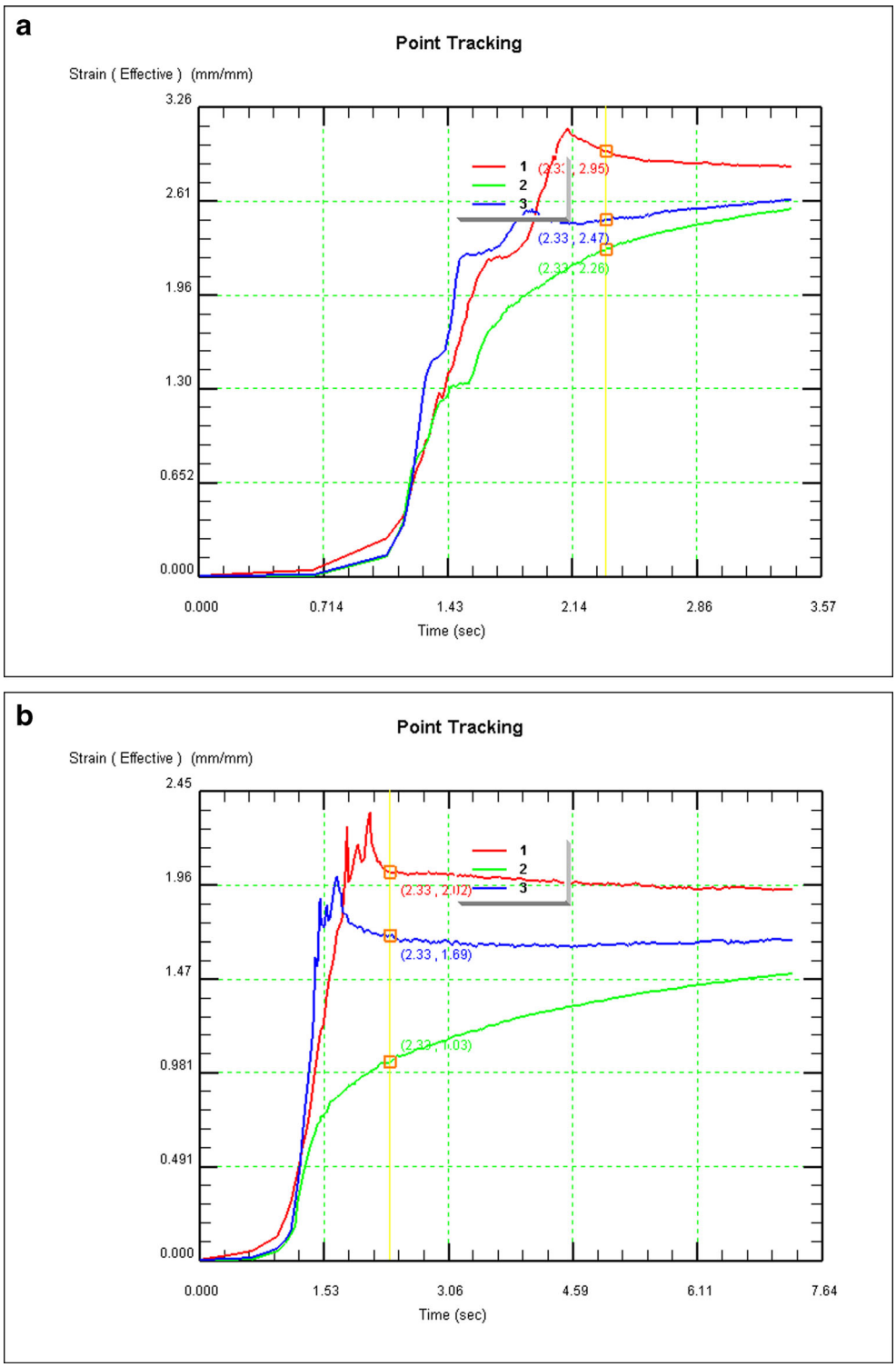

Fig. 5 **a** Selected points in the longitudinal section of billet, the strain evolution of three points with extrusion temperature 370 °C for the **b** ES process and **c** direct extrusion, respectively

in Fig. 5b, c. It is clear that effective strains of these points increase rapidly from 0 to 1.47–2.45 from extrusion time 0 to 1.32 s during direct extrusion. During subsequent continuous shearing period, effective strains of point p2 increase slowly to 2.5, but the strains increase to 2.85 and 2.6 for p1 and p3, respectively. It is obvious that strain evolutions of the inner billet are larger than those of other positions. When the plastic deformation is steady, the strains increase slowly. When the AZ31 magnesium alloy flows into the severe deformation zone, severe deformation occurs.

3.3 Stress distribution for different deformation paths

The stress distributions of the longitudinal section in rods at 370 °C for the direct extrusion and the ES process with an extrusion ratio of 12 are shown in Fig. 6, respectively. Maximum stresses caused by the ES process are bigger than those caused by direct extrusion. During direct extrusion, effective stresses of these points as shown in Fig. 6a are about 322 MPa during the end of the shear period, which indicates that the shear stresses

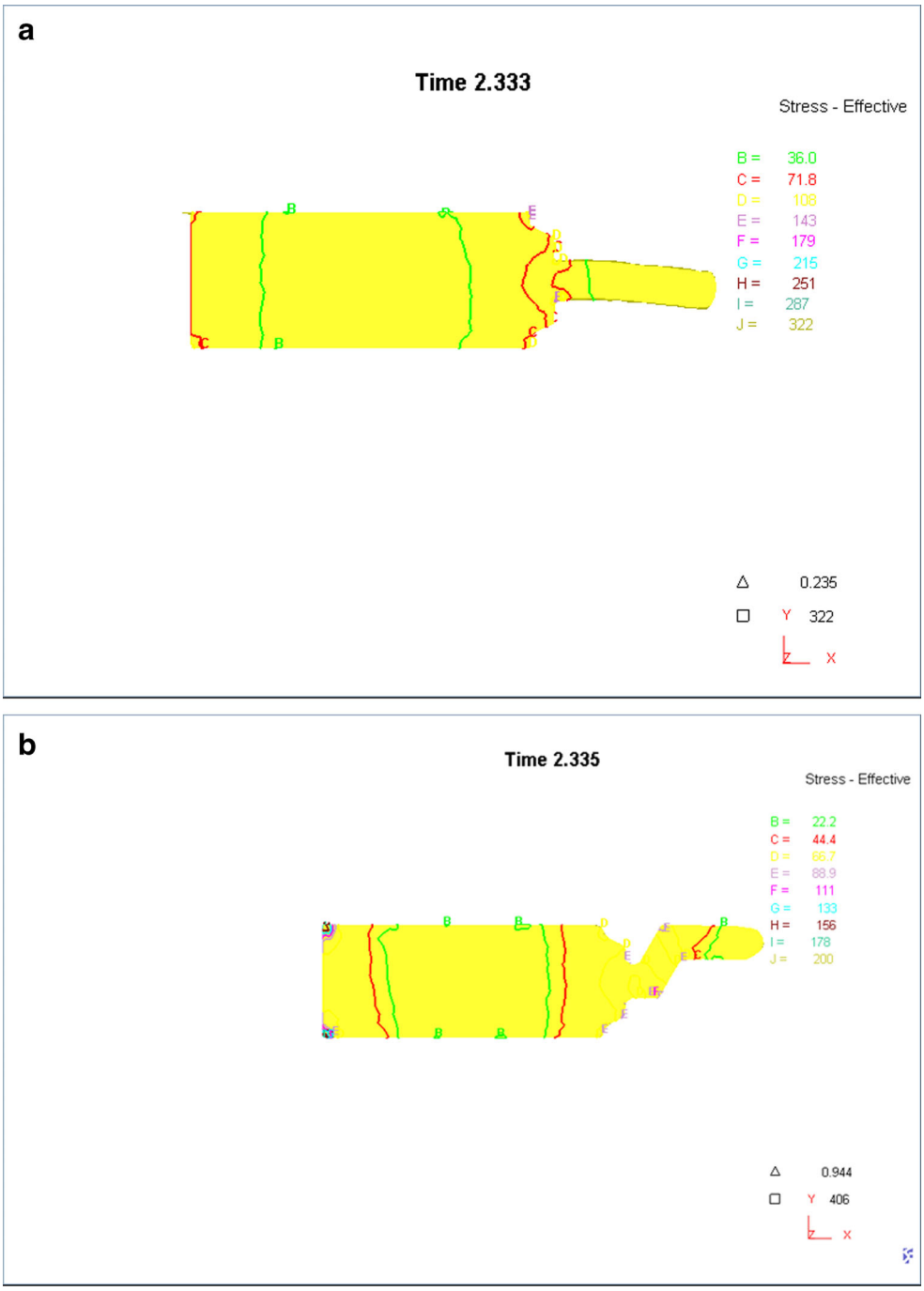

Fig. 6 The stress distributions of longitudinal section in rods at 370 °C for the direct extrusion (**a**) and the ES process (**b**), respectively

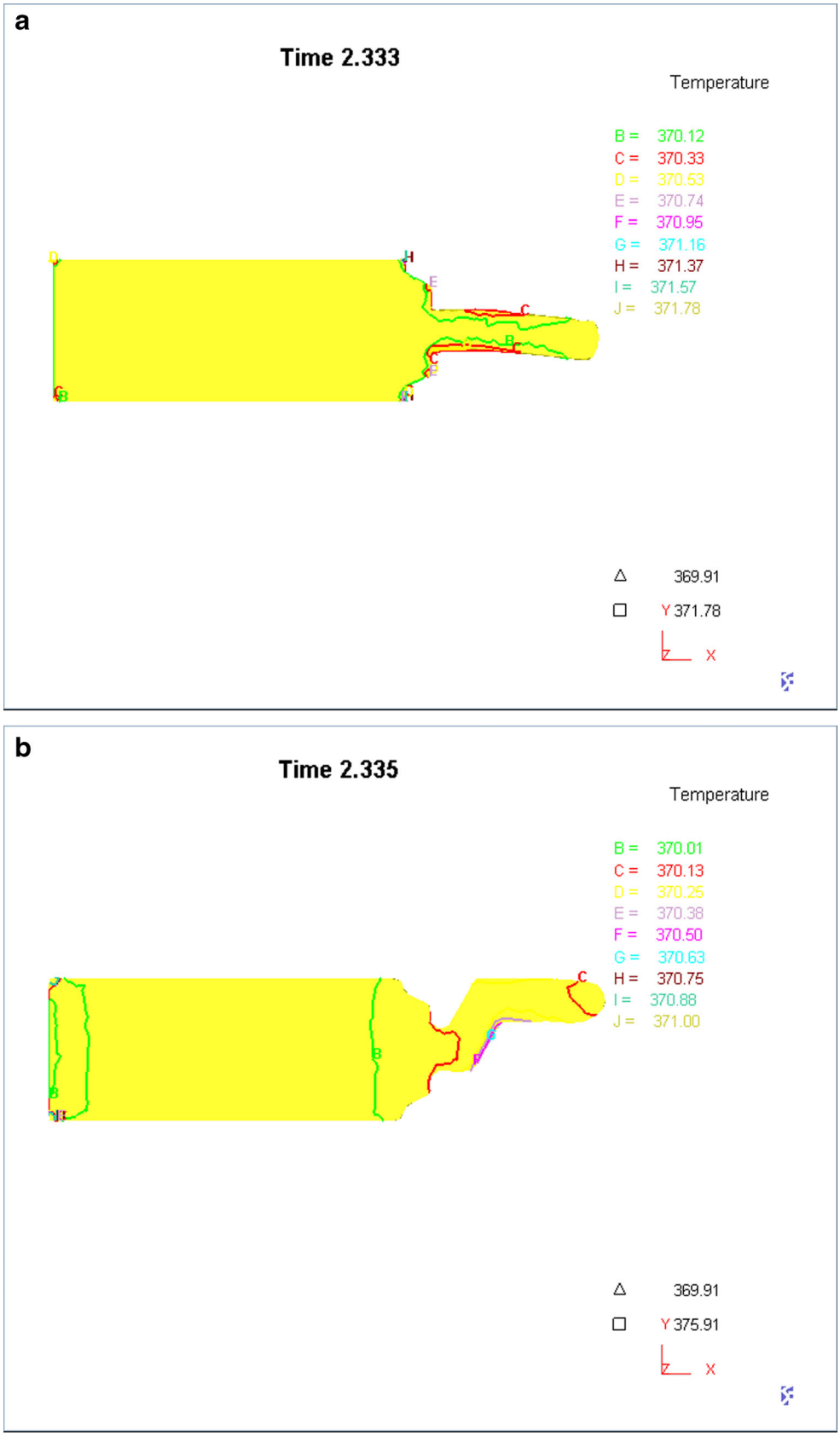

Fig. 7 The temperatures distributions of longitudinal section in rods with a billet temperature 370 °C for the direct extrusion (**a**) and the ES process (**b**), respectively

locate concentricity in the deformation zone of the direct extrusion die or ES die, and the effective stress increases as big as 406 MPa during the ES process.

3.4 Temperature distribution for different deformation paths

The temperature distributions of longitudinal section in rods with a billet temperature of 370 °C for the direct extrusion and the ES process are shown in Fig. 7a, b, respectively. It is obvious that the temperatures of rods extruded by the ES die are bigger than those which are formed by direct extrusion at the extrusion time of 2.33 s. The temperature distributions for different dies are significantly different and not even. The deformation of the initial extrusion is nonuniform, and the highest temperature is 371.78 °C in Fig. 7a, but the value is 375.9 °C in Fig. 7b. The shear deformation can be obtained at the intersection of the two channels. Distributions of the isotherms are lamellar in the deformation zone. The deformation of this zone is close to the simple shear deformation.

The curves of maximum temperatures varying with extrusion time for the direct extrusion and ES processes are shown in Fig. 8. It is clear that the maximum temperature of the rod increases continuously with the development of the ES process and direct extrusion. It is noticed that the increases of maximum temperature for the two different deformation paths predicted by the finite element simulations are significant. It is clear that the maximum temperatures during the ES process are higher than those of direct extrusion. The factors to increase the temperature during the ES forming are (1) heat transfer from the die and punch, (2) friction between the rod material and die, and (3) plastic deformation during the ES forming process. The reason for the lower temperature increments for direct extrusion is mainly due to lower temperature gradient between the die and billets. Since the temperature rise depends on the heat generated within the deformation zone, heat generation depends on the internal power of deformation and frictional power.

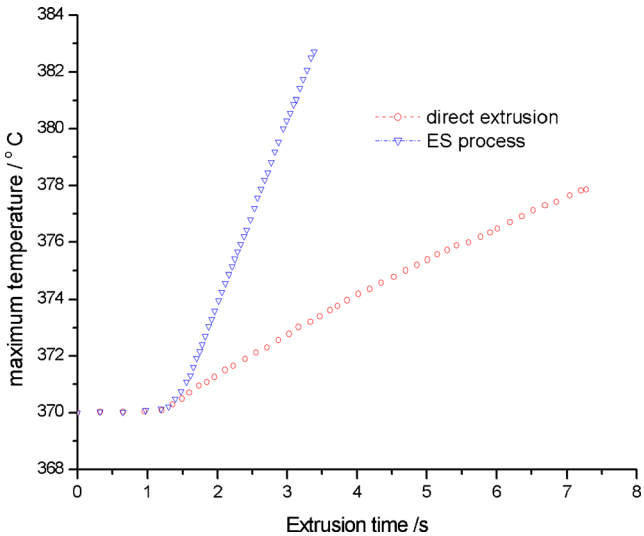

Fig. 8 Curves of the maximum temperatures with extrusion time for the ES process and direct extrusion

3.5 Microstructure observations for different deformation paths

The microstructures in longitudinal sections of the extruded rods at the extrusion temperature of 370 °C with direct extrusion and ES extrusion, respectively, can be seen in Fig. 9. In Fig. 9a, there are many original grains, and the sizes are as big as 80 μm, and the size of fine grains is around 5 μm, so the part dynamic recrystallization happen, and the distribution of grains is nonhomogeneous.

There are almost equiaxed grains in ES hot-extruded rods as shown in Fig. 9b. After the hot ES process, grains are refined and more homogenous. It is clear that the average sizes of microstructures for magnesium alloy prepared by the ES process are finer than those produced by direct extrusion [6]. The grain sizes of recrystallized structure in the ES

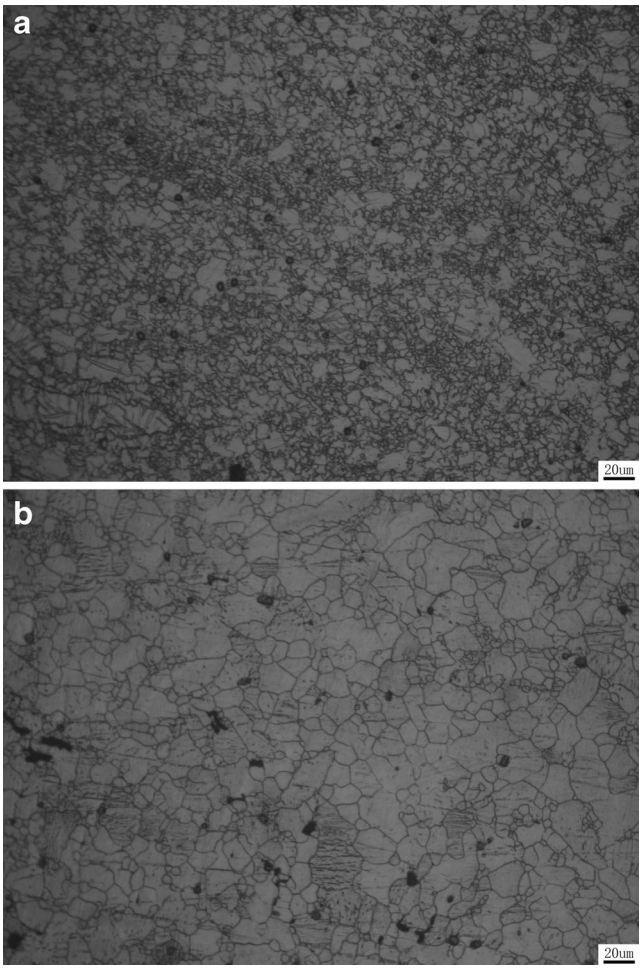

Fig. 9 The microstructures in longitudinal section of the extruded rods with an extrusion temperature 370 °C for direct extrusion (**a**) and ES process (**b**), respectively

process are approximately 2–3 μm, while those fabricated by direct extrusion are approximately 4–5 μm. This is because the ES process included two simple shear extrusion processes more than an ordinary extrusion. It can be found that the microstructures of longitudinal section for ES and the direct extrusion are part recrystallization microstructures with an extrusion ratio of 12. The ES process includes two simple shear extrusion processes more than an ordinary extrusion. The shear deformation might cause more shear strains and stresses in the magnesium alloys. The original large grains in as-cast magnesium alloy are rotated and broken by the extrusion force and extrusion die, and dynamic recrystallization occurred in local regions under the external forces and bigger cumulative shearing strains and stresses accompanying small equiaxed grains around the original grains. But the recrystallized grains are uneven, and there exist a small amount of fibrous microstructures.

The Levy–Mises flow rule can be used to relate the stress to the strain rate during bulk metal forming. This flow rule is shown in Eq. (3). The equation describes the relationship between the stress and strain rate [10].

$$\sigma_{ij} = \frac{1}{\dot{\lambda}}\dot{\varepsilon}_{ij} \tag{3}$$

where σ_{ij} and $\dot{\varepsilon}_{ij}$ are flow stress and strain rate for point ij, respectively. The coefficient λ is a constant.

Deformation paths would affect the amount of flow stress. The incremental shearing of magnesium alloy would increase strain rates and stress in the magnesium alloy.

The strain rates ε_1 of two shearing for the ES process are described in Eq. (4) [11, 12].

$$\dot{\varepsilon}_1 = \left[\frac{2\cot\left(\frac{\phi}{2}+\frac{\psi}{2}\right)+\psi\csc\left(\frac{\phi}{2}+\frac{\psi}{2}\right)}{\sqrt{6}}\right]\frac{\sqrt{v_2}}{\psi R_2}\exp\left(\frac{Q}{RT}\right) \tag{4}$$

where $\varnothing$ is the channel angle, ψ is the outer channel angle, V_2 is the extrusion velocity during two shearing period, R_2 is the radius of extruded rod, Q is the activation energy, R is the gas constant, and T is the extrusion temperature.

The relationship between the average recrystallization grain size (d) and the Zener–Hollomon parameter (Z) during dynamic recrystallization is given by Eq. (5) [13].

$$\left(\frac{d}{d_0}\right)^n = 10^{-3}\times Z^{-1/3} \tag{5}$$

The temperature-corrected strain rate Z is given by Eq. (6) [14–17].

$$Z = \varepsilon\exp\left(\frac{Q}{RT}\right) \tag{6}$$

where $\dot{\varepsilon}$ is the strain rate, Q is the activation energy for the deformation, T is the temperature, and R is the gas constant.

It can be seen from the Eqs. (4), (5), and (6) that average sizes of magnesium alloy decrease with the rise of strain rates. The effective strain rates decrease with the rise of channel angles. It is obvious that the average sizes of grains fabricated by the ES process are finer than those prepared by direct extrusion.

4 Conclusions

A full 3D FEM simulation and experiments of as-cast AZ31 magnesium alloy billet subjected to the ES process and direct extrusion have been carried out successfully. Numerical and experiments have helped in a big way to understand the deformation behavior of AZ31 magnesium alloy during the ES process. The evolution of extrusion forces for the ES process and direct extrusion process has been analyzed using the computer numerical simulation, and the ES process could be divided into four stages. The loads of the ES process increase obviously compared with those of direct extrusion. The strains increase with the ES process progressing. Strains and stresses caused by the ES process are bigger than those caused by direct extrusion. Maximum temperatures during the ES process are higher than those of direct extrusion. The microstructure of AZ31 magnesium alloy billet in the ES and the direct extrusion with an extrusion ratio of 12 have been observed and analyzed, and compared. It might be reasonable to conclude that the effect of the microstructure refinements of magnesium alloy by the ES process is remarkable. The recrystallized microstructures formed in the ES process are more uniform and finer than those fabricated by direct extrusion. The ES process can be an effective grain refinement method—not only grains of the rod surface can be refined, but also grains of the center has also been refined.

Acknowledgments This work is supported by the open fund for Key Laboratory of Manufacture and Test Techniques for Automobile Parts (Chongqing University of Technology) Ministry of Education in 2003 and by the National Science Foundation for Young Scholars of China (Grant No. 51101176) and foundation of postdoctorate in Chongqing City (Project Number Xm201327), and China Postdoctoral Science Foundation funded project.

References

1. Segal VM et al (1981) Plastic working of metals by simple shear. Russ Metall 1:99–105
2. Zhernakov VS, Stol Yarov VV et al (2001) The developing of nanostructured SPD Ti for structural use. J Scr Mater 44(8-9): 1771–1774
3. Gong X, Li H, Kang SB, Cho JH, Li S (2010) Microstructure and mechanical properties of twin-roll cast Mg-4.5Al-1.0Zn alloy sheets processed by differential speed rolling. Mater Des 31(3):1581–1587
4. Gong X, Kang SB, Li S, Cho JH (2009) Enhanced plasticity of twin-roll cast ZK60 magnesium alloy through differential speed rolling. Mater Des 30(9):3345–3350

5. Hu HJ, Huang WJ (2013) Effects of turning speed on high-speed turning by ultrafine-grained ceramic tool based on 3D finite element method and experiments. Int J Adv Manuf Technol 67(1–4):907–915
6. Hongjun H, Dingfei Z, JunPing Z (2010) Microstructures in an AZ31 magnesium alloy rod fabricated by a new SPD process based on physical simulator. Trans Nonferrous Met Soc China 3:478–483
7. Hongjun H, Dingfei Z, MingBo Y, Ming D (2011) Grain refinement in AZ31 Magnesium alloy rod fabricated by an ES SPD process. Trans Nonferrous Metals Soc China 21(2):243–249
8. Hongjun HU, Zhang D, Fusheng PAN, Mingbo YANG (2009) Analysis of the cracks formation on surface of extruded magnesium rod based on numerical modeling and experimental verification. Acta Metall Sin (Engl) 22(5):353–364
9. Hongjun HU, Dingfei ZHANG, Fusheng PAN (2009) Computer simulation and optimization of equal channel angular extrusion of AZ31 magnesium alloy. Mater Sci Forum 610–613:780–782
10. Hu HJ, Huang WJ (2013) Studies on wears of ultrafine-grained ceramic tool and common ceramic tool during hard turning using Archard wear model. Int J Adv Manuf Technol 69(1–4):31–39
11. Hadadzadeh A, Wells MA, Jayakrishnan V (2014) Development of a mathematical model to study the feasibility of creating a clad AZ31 magnesium sheet via twin roll casting. Int J Adv Manuf Technol. doi: 10.1007/s00170-014-5831-6
12. Mofid MA, Abdollah-zadeh A, Hakan Gür C (2014) Investigating the formation of intermetallic compounds during friction stir welding of magnesium alloy to aluminum alloy in air and under liquid nitrogen. Int J Adv Manuf Technol 71(5–8):1493–1499
13. Feng F, Huang S, Jianhua H, Meng Z, Lei Y (2013) Analysis of the bulging process of an AZ31B magnesium alloy sheet with a uniform pressure coil. Int J Adv Manuf Technol 69(5–8):1537–1545
14. Rajakumar S, Razalrose A, Balasubramanian V (2013) Friction stir welding of AZ61A magnesium alloy. Int J Adv Manuf Technol 68(1–4):277–292
15. Wu G, Hu H, Gong X, Zhang W, Wang K, Dong T (2007) Application and development of casting process parameterized graph library based on AutoCAD software. Foundry Technol 28(4):535–537
16. Chung YH, Park JW, Lee KH (2006) An analysis of accumulated deformation in the equal channel angular rolling (ECAR) process. Mater Inter 12(4):289–293
17. Hu H, Yang M, Gong X, Li G (2006) Optimization of casting processes based on computer numerical simulation. Ordnance Mater Sci Eng 29(6):51–53